Slow Wave Oscillation reveals the discrete segregation of dorsal striatum

J. Alegre-Cortés*, M. Sáez*, R. Montanari, R. Reig

Affiliation
Instituto de Neurociencias CSIC-UMH, San Juan de Alicante, Spain

*Equal contributions.
Corresponding Author: Ramón Reig ramon.reig@umh.es

Keywords
Striatum/ Corticostriatal connectivity/ Dorsomedial/ Dorsolateral/ Beta oscillations/ Circuits segregation/*In vivo* patch-clamp/ NA-MEMD

Abstract

Behavioural studies differentiate the rodent dorsal striatum (DS) into lateral and medial regions based on their particular roles; however, anatomical evidence suggest that it is a unified structure. To understand striatal dynamics and basal ganglia functions, it is essential to clarify if this behavioural-based segregation is supported by two different circuits. Here, we show that the mouse DS is made of two non-overlapping functional circuits divided by a sharp boundary. Combining *in vivo* optopatch-clamp and extracellular recordings of spontaneous activity, we demonstrate different coupling of lateral and medial striatum to the cortex together with an independent integration of the propagated activity, due to particular cortico-striatal connectivity and local attributes of each region. Additionally, differences between striatonigral and striatopallidal neurons were detected only in the lateral DS. These results demonstrate that the rodent DS is segregated in two neuronal circuits, suggesting its homology with the caudate and putamen nuclei of primates.

Introduction

The basal ganglia are involved in a diversity of functions including motor control, learning, decision making and reward [1-3]. The striatum is the main input structure of the basal ganglia, receiving glutamatergic transmission from the cortex and the thalamus[4-8]. In primates and other mammals, the dorsal part of the striatum is formed by the nuclei caudate and putamen, which are anatomically separated by the internal capsule. In contrast, rodent dorsal striatum (DS) is considered a homogeneous structure due to the absence of anatomical border and the copious presence of overlapping axonal connections[4,7,8]. Accordingly, a large number of DS studies followed this anatomical perspective, assuming homogeneous neuronal and microcircuit properties along the rodent dorsal striatum. However, a growing body of knowledge has divided the DS in two regions, dorsomedial (DMS) and dorsolateral (DLS) striatum, based on their different behavioural roles[9,10]. While both regions participate in motor control, DLS mediates habit, stimulus-response associations and navigation, whereas the DMS regulates action-outcome associations, goal-directed strategy, flexible shifting between behavioural strategies and, in general, supports higher cognitive behaviours[2,11,9]. Therefore, in order to understand the basal ganglia circuits and their related behaviours, an essential question remains: Is the functional segregation of the dorsal striatum supported by two different circuits?

Cortical axonal projections enter the basal ganglia through the striatum, forming organized glutamatergic synapses along its mediolateral axis, and defining multiple striatal subregions[5]. This corticostriatal axonal innervation presents a high degree of convergence and divergence[12,4] and originates in both hemispheres from different sub-types of pyramidal neurons[7,13]. Corticostriatal connections innervate both striatonigral and striatopallidal medium-sized spiny neurons (direct and indirect MSNs respectively), which represent 95% of the neurons in the striatum[6], and different types of interneurons[14]. DLS is highly innervated by axons from somatosensory and motor related cortical areas, while DMS receives cortical axons from visual, auditory, associative, limbic[5,7] and somatosensory cortical regions, although the latter projections are of lower axonal density compared with DLS[10].

In addition to the differences on cortical or thalamic axonal innervation, there are dissimilarities on the composition of the striatal microcircuits. The distribution of parvalbumin (PV) and cholinergic (ChI) interneurons along the mediolateral axis of the DS is not homogeneous[15,16,17]. Furthermore, dopaminergic projections from the lateral part of the substantia nigra massively innervate DS[18], mostly impacting the activity of ChIs[19]. All these precise afferent connectivity, microcircuit interactions and neuromodulation regulate the synaptic activity of DLS- and DMS-MSNs.

The activity of every neural circuit in the brain is limited by anatomical and functional constrains[20] which will restrict the repertoire of spontaneous and evoked activity patterns[21]. In this work, we describe how DLS and DMS circuits can be segregated based on their spontaneous activity and propose a biological substrate that explains their differences.

As a model of spontaneous activity we used the Slow Wave Oscillation (SWO)[22]. This

brain state is characterized by periods of high synchronized spontaneous neural activity (Up states) intermingled with periods of silence (Down states) at ~1Hz[22,23]. The SWO is originated in the cortex and propagates directly to the striatum, modulating the resting state of MSNs[24,25] and interneurons[10].

In this work, we show how the dorsal striatum is divided in two non-overlapping circuits, based on their spontaneous activity. In addition, we describe differences in the beta oscillations and in the intrinsic properties of the MSNs of these circuits, as well as in the direct and indirect pathways. In conclusion, our results demonstrate that dorsal striatum is divided in two functional circuits, separated by a sharp boundary, each of them with specific properties that are essential to understand the striatum and basal ganglia functions.

Results

Sequential propagation of the cortical SWO to the striatum

We obtained *in vivo* whole-cell patch-clamp recordings from 223 neurons under anaesthesia, located in dorsal striatum lateral, central or medial regions and cortex (see methods). At the same time, double cortical LFP recordings were performed (Fig. 1a). Additionally, 6 pairs of MSNs (n=12, 6 DLS-, 6 DMS-MSNs) were recorded simultaneously in DS. Example of recovered MSNs are presented in Fig. 1b. All the recorded cortical and striatal neurons displayed SWO with prominent Up-Down states (Fig. 1c-e, 2a, 4a-b, 4d, 5a, 6a, S1, and S3) as previously described[25,10]. Striatal neurons displayed a very low rate of spontaneous action potentials (DLS-MSNs=0.3±0.95 Hz, DMS-MSNs=0.24±0.53 Hz) restricted to the Up states. We analysed the intrinsic properties of MSNs between striatal regions and DLS-MSNs showed higher capacitance and resistance than DMS-MSNs (Table 1).

To understand if DLS and DMS neurons could have different properties in their SWO patterns, we first studied their correlation with several cortical regions (Fig. 1). We applied the Noise-Assisted Multivariate Empirical Mode Decomposition (NA-MEMD) to extract the Intrinsic Mode Function (IMF) [see Methods] carrying the information about the SWO (Fig. 1c) and used it to compute the cross-correlation between the whole-cell recordings of the MSNs in DLS or DMS with the pairs of simultaneous LFPs recorded in different cortical regions (FrA, M1, S1, V1) (Fig. 1d-f). We found that neuronal activity from DLS- and DMS-MSNs had different correlations with FrA, M1 and V1 LFPs (Fig. 1g). Correlation with FrA and M1 activity was higher for DLS neurons, while correlation with V1 was higher for neurons recorded from DMS, consistent with results obtained from visual stimulation[10]. When we represented correlation values with FrA and V1, two clusters were clearly distinguishable, corresponding to DMS- and DLS-MSNs (Fig. 1i), suggesting specific functional coupling to the cortex for both striatal areas.

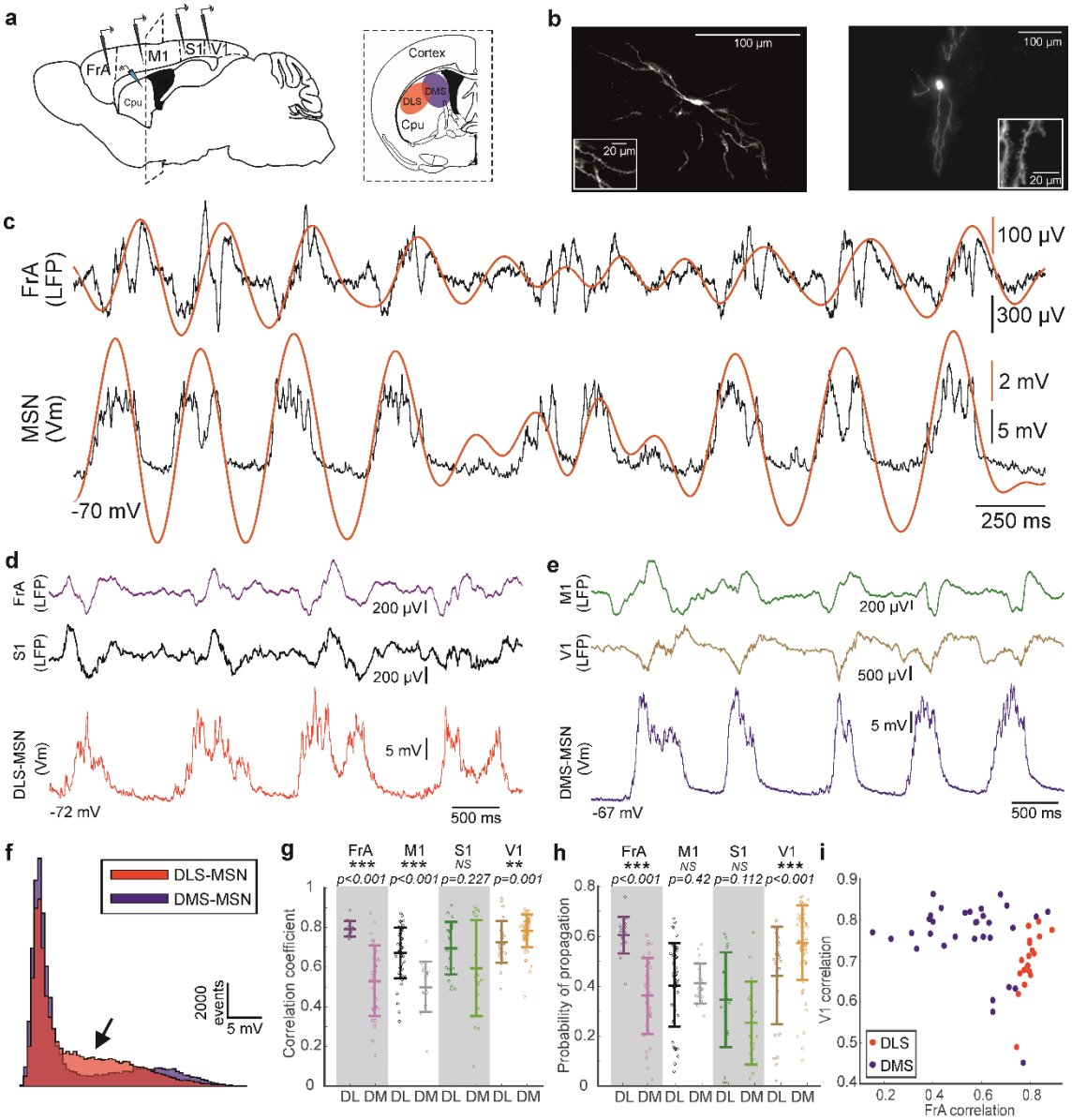

Figure 1. Integration of the SWO in dorsal striatum. a, Schematic representation of the *in vivo* recording setup. **b,** Morphological reconstruction of a DLS- (left) and DMS- MSN (right). Different scales show neuron magnitude and its dendritic spines, confirming that the recorded neuron is a MSN. **c,** Representative LFP (top) and whole-cell patch-clamp recording of a MSN (bottom), together with SWO extraction by NA-MEMD (orange line) **d,** Example of simultaneous recordings from a DLS-MSN (red) and double LFPs from FrA (purple) and S1 (black). **e,** Example of simultaneous recordings from a DMS-MSN (blue) and double LFP from M1 (green) and V1 (ochre). **f,** Histogram of the membrane potential values of the MSNs in d and e, the back arrow indicates the dissimilar shape of the bimodal distributions**. g,** Probability of propagation of the Up state from different cortical regions to DLS- and DMS-MSNs. **h,** Correlation coefficient of different cortical regions to DLS- and DMS-MSNs. **i,** Raster plot showing the correlation between all MSNs and the LFP from FrA and V1.

Next, we analysed the probability of occurrence a striatal Up state, recorded in a MSN, after the occurrence of a cortical Up state (Fig. 1h). Consistent with the correlation results, the probability that an Up state in FrA is followed by an Up state in DLS was significantly higher than in DMS. Similarly, Up states in V1 had higher probability to follow an Up state in DMS than in DLS. In summary, these results show different levels of SWO

correlation and propagation with multiple cortical regions for DMS- and DLS-MSNs, suggesting different functional connectivity of each striatal region with the cerebral cortex[20].

Consistent with the described propagation of the SWO across the cortex[26], a sequential activation can be expected along the DS. To test this hypothesis, we first computed the occurrence within the cortex, between Up states recorded by the LFPs in V1 and FrA. These two regions are placed at opposite poles of the cortex and thus are appropriate to study the sequential occurrence of the SWO. When an Up state was recorded in FrA and V1, there was a significantly higher chance that the Up states were recorded in FrA before V1 (72%, p value< 0.0001, data not shown).

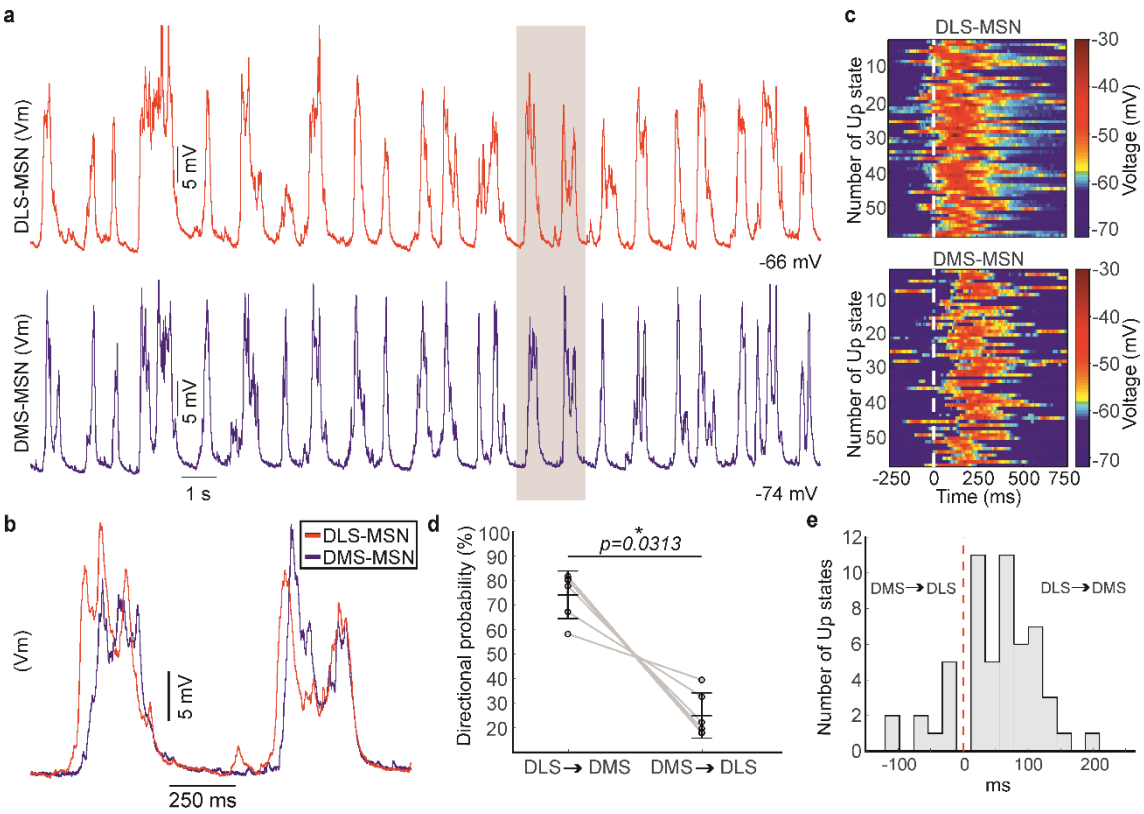

Figure 2. Directionality of the SWO in dorsal striatum. a, Representative example of simultaneous paired *in vivo* whole-cell recordings in DLS (top, red) and DMS (bottom, blue). **b,** Inset of the shaded part in a showing two aligned traces to its Down states voltage of the simultaneous *in vivo* paired recordings. Notice that DLS-MSN onset is preceding the DMS-MSN. **c,** Raster plot of a representative example of a paired recording in DLS (top) and DMS (bottom) MSNs. Each line represents a 1 second time window aligned to the onset of each of the Up states of the DLS-MSN (white line). **d,** Directional probability of DS MSNs. **e,** Example of the distribution of delays between the onset of the Up state in the DMS- relative to the DLS-MSN. Positive values indicate that the Up state arrive later to the DMS-MSN. Same neuron in a, b, c and e.

Finally, we performed simultaneous whole-cell patch-clamp recordings of two MSNs, located in the DLS and DMS (Fig 2a). In all recorded pairs, the Up state in DLS-MSN preceded the one in the DMS-MSN (Fig 2b-d) for several tens of milliseconds (47.69±30.06 ms, representative example in Fig 2c). On average, 74% of the Up states

evoked in both MSNs arrived first to the DLS (p value=0.0303, Fig 2d). This ratio is consistent with the values computed using pairs of LFPs in cortex described above. Fig. 2b-c and 2e show a representative example of the propagation delay to the pair of recorded MSNs. When we compared the onset times of both whole-cell recordings, a delay of the DMS-MSN was evident (Fig. 2e), demonstrating a clear sequential generation of the Up states in the DS.

Our previous results regarding the propagation of the SWO (Fig 1g,h), together with a similar directionality of propagation from FrA to V1 and DLS to DMS confirm a stronger functional coupling of FrA to DLS and V1 to DMS.

Dorsal striatal regions can be identified by their SWO properties

To understand the differences between DLS and DMS circuits, we characterized the SWO properties in whole-cell recordings from DS-MSNs. We computed 13 different features (Fig. 3a), of which 11 were statistically different between DLS- and DMS-MSNs. The average voltage in the Up states was higher in the DMS-MSNs, as well as their Up state standard deviation, minimum and maximum voltage during Up state and the total amplitude of the Up states. The upward and downward Up states transitions slopes as well as its ratio were also higher in DMS-MSNs. DLS-MSNs displayed longer Up states, higher peak to peak amplitude and higher number of peaks during the Up states [all features are explained in methods section].

Next, we searched for those features whose combination maximized the differences between SWO from DLS- and DMS-MSN, measured as the accuracy of classifying MSNs corresponding to each circuit. To this aim, we performed a Recursive Feature Elimination (RFE) to rank the 13 computed features according to their combined utility to classify DLS- or DMS-MSNs, using a Support Vector Machine (SVM) with a linear kernel (Fig. 3b). The most relevant features were 1- the number of peaks and 2- the amplitude inside the Up state, which resulted in an accuracy score of 84.61±0.47% (Fig 3b-d). When a third feature, the speed of transition from up to Down states, was added, the accuracy increased to 88.56±0.57% (Fig. 3b-d). The addition of new parameters increased the accuracy up to ~92%, value at which accuracy remained stable (Fig. 3b). In a compromise between accuracy and interpretability, we selected the space formed by the three most relevant features for further analyses (Fig. 3e). We performed an additional control analysis in which we classified the MSNs recorded from each animal as test set, using the remaining MSNs as training set. The accuracy following this calculation was 88.89% (Supplementary Fig. 4), excluding the presence of inter-animal bias. In summary, our classifier based on the SWO of the MSNs indicates that DLS and DMS are identified as two distinct functional circuits.

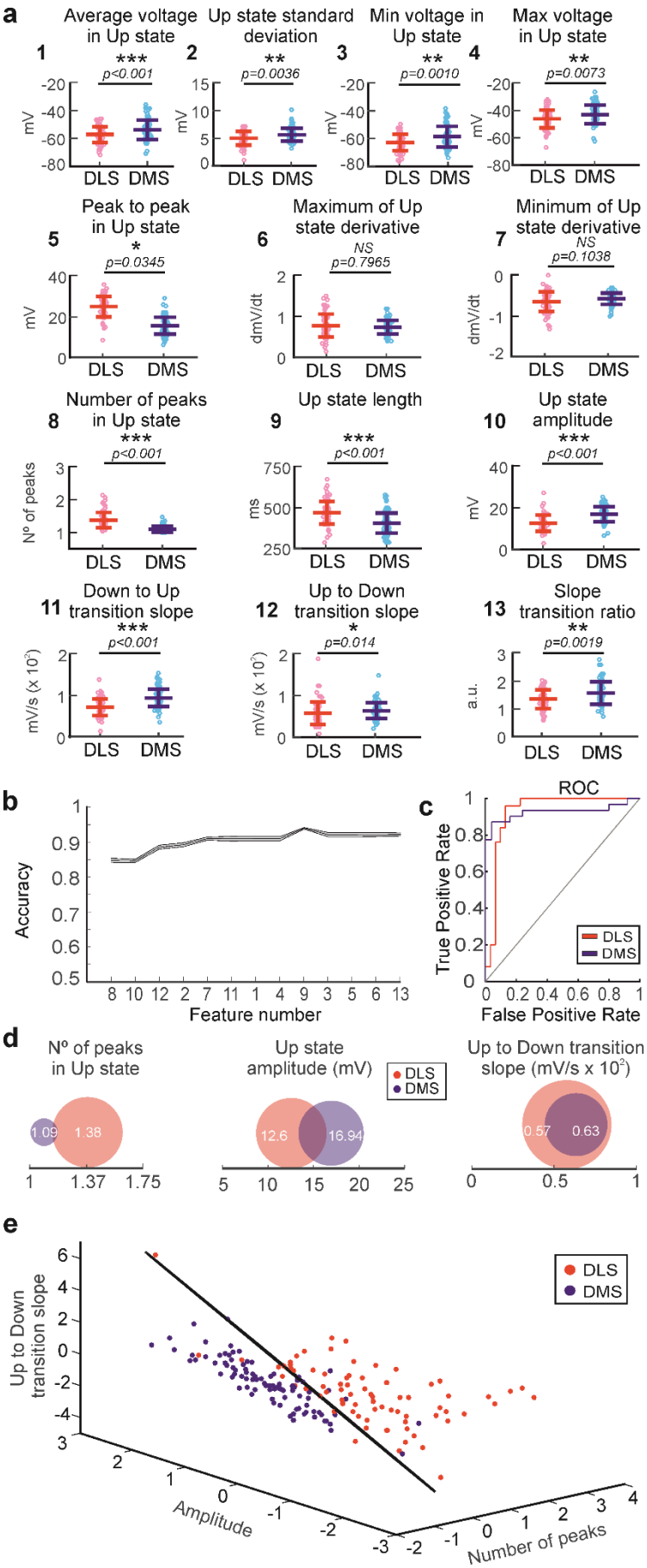

Figure 3. Featurization and classification of SWO in dorsal striatum. a, Featurization of the SWO of DLS- and DMS-MSNs [See methods]. **b,** RFE of the computed features (feature number) to determine their order of relevance classifying DLS- and DMS-MSNs. A SVM with a linear kernel was selected as classification algorithm. **c,** Example ROC curve of the DLS-DMS classification for one of the cross-validations using the 3 most relevant features. **d,** Schematic representation of the data distribution of DLS and DMS groups for the most relevant features (numbers 8, 10, and 12). **e,** Subspace of classification based on the RFE results. Dots represent individual MSNs recorded in DLS (red) or DMS (blue). Classification hyperplane obtained after training the SVM with linear kernel in black.

To understand the main source of differences between the DLS and DMS SWO, we started by analysing the first ranked feature, number of peaks during Up states (Fig. 4a). We studied whether similar differences occurred in cortical regions, from where they can be inherited by the dorsal striatum. We performed *in vivo* whole-cell patch-clamp recordings in Layer V of FrA, M1, S1 and V1 cortices (Fig. 4b) and found that S1 and M1 have significantly higher average number of peaks per Up state than FrA and V1 (Fig. 4c). FrA also displays a significantly higher number of peaks than V1. FrA sends abundant projections to DLS, while their projections to DMS are scarce[5]. This result suggests that, while the transition to the Up state of the SWO in DLS is triggered by more frontal cortical regions (Fig. 1g-i), the activity during the Up state may be governed by sensory-motor regions.

The main features for the classification of DLS- and DMS-MSNs were relative to state transitions (Up to Down transition) or intra-state transitions (number of peaks). In order to understand whether these differences may be caused by changes in the depolarizing and hyperpolarizing dynamics of MSNs during the SWO cycle, we studied the temporal properties of the voltage transitions. To analyse the convergence of synchronized hyper/depolarizing events onto MSNs that created detectable changes in the whole-cell recording, we detected the sharp transitions of the voltage trace and phase locked them to the SWO cycle [see methods]. Thus, we obtained an approximate measure of the temporal dynamics of hyper/depolarizing events of the MSNs during the SWO. Then, we computed their ratio for the DLS- and DMS-MSNs. We found differences in the depolarizing/hyperpolarizing ratio (DH ratio) of DLS- and DMS-MSNs aligned to the transitions between Up and Down states (Fig. 4e). The DH ratio was significantly shifted toward excitation for DMS-MSNs during the transition from the Down to the Up state and shifted toward hyperpolarizing events during the transition from the Up to the Down state. This is consistent with the significant differences found for both Up states slopes (Fig. 3a).

Characterization of the fast spontaneous activity.

High frequency oscillations are prominent during behaviour, but also appear during the Up states of the SWO[27]. In the cortico-basal ganglia-thalamic loop, high frequency activity has been related with different functions and processes in health and disease[28,29]. We compared the energy in the theta (6-10 Hz), beta (10-20 Hz) and gamma (20-80 Hz) bands of DLS- and DMS-MSNs (Fig. 5a, Supplementary Fig 3a-d). Our results show that the energy of the beta band was slightly higher, and statistically different, in DMS-MSNs (Fig. 5b,e). On average, the peak of beta energy occurs in the first third of the Up state in both striatal regions, but it is closer to the beginning of the Up state for DMS-MSNs (Fig. 5d, DMS=-26.81±24.63º, DLS=-13.26±30.01º, where 0º is the centre of the Up state).

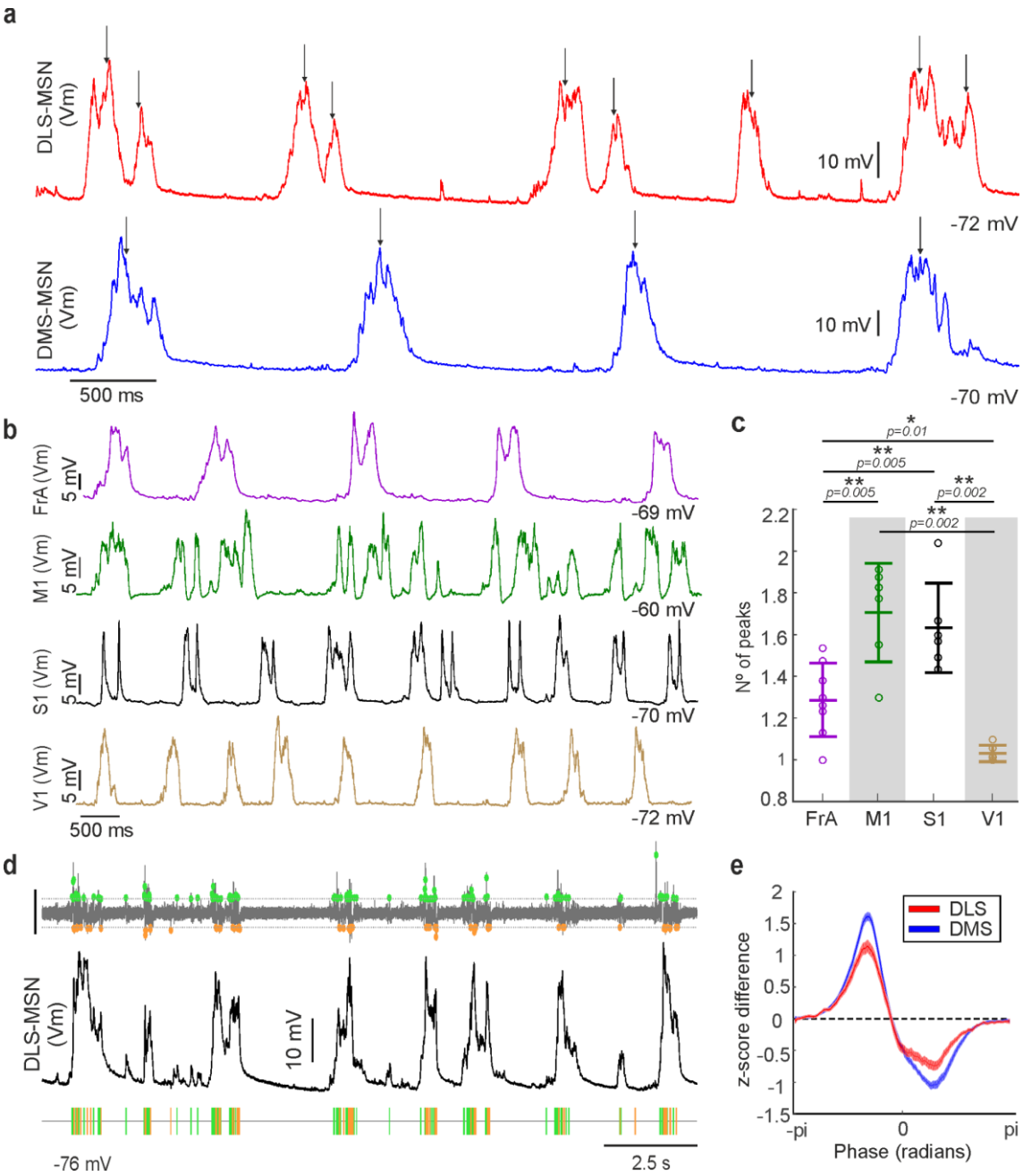

Figure 4. Number of peaks and depolarized/hyperpolarized ratio of the SWO in dorsal striatum. **a,** Detection of peaks (black arrows) in the Up state in a DLS-MSN (red) and a DLS-MSN (blue) [See methods]. **b,** Representative examples of SWO in different cortical regions. **c,** Number of peaks per Up state in the different cortical regions. Non-labelled comparisons are not significant. **d,** Extraction of depolarized/hyperpolarized events by computational approach [see methods]. Top: Detection of the events using a threshold in the first derivative of the Vm. Scale bar represents 0.1 dmV/dt. Bottom: Representation of the detected depolarized (green) and hyperpolarized (orange) events from whole-cell recording of a DLS-MSN (middle). **e,** Average of the depolarized/hyperpolarized ratio aligned to the SWO cycle of DMS- and DLS-MSNs.

Then, we asked whether the difference in beta energy between DMS- and DLS-MSNs could be inherited from the cortex. We computed the beta energy of the membrane voltage of the recorded neurons and compared them between the cortical regions (FrA, M1, S1,

V1). We did not find significant differences in the energy of the beta band in any cortical region (Fig. 5c).

Finally, we tested if high frequency oscillations contained enough information to classify DMS- and DLS-MSNs. To that end, we trained an SVM with a linear kernel, as it was performed with the previous SWO features. We obtained an accuracy of 60.19±10.81%, suggesting that the energy at high frequencies during Up states do not contribute to discriminate between DMS- and DLS-MSNs.

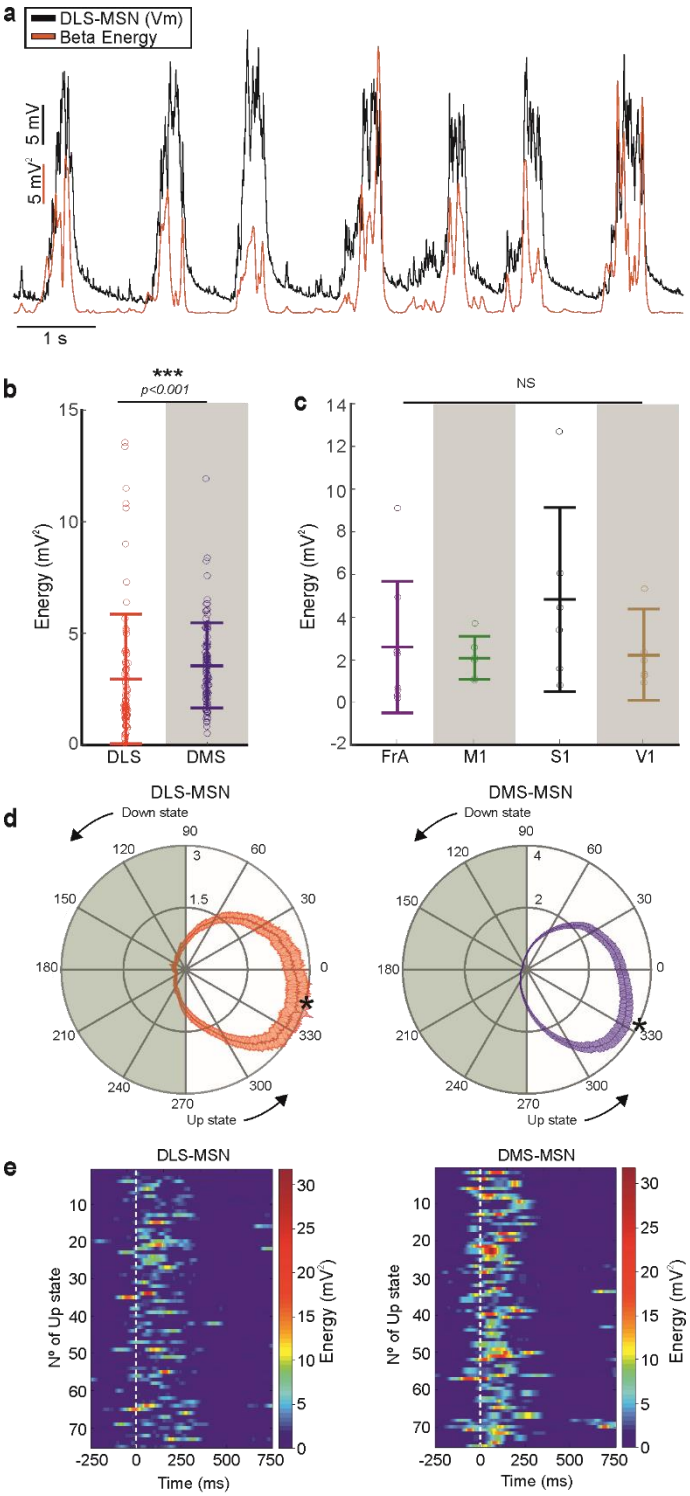

Figure 5. Beta band in membrane voltage of dorsal striatal MSNs. a, Example of energy of the beta band (red trace) during the MSN SWO recorded in DMS. **b,** Energy of the beta band of DLS- and DMS-MSNs. **c,** Energy of the beta band of neurons recorded on layer V in FrA, M1, S1 and V1. **d,** Average of phase alignment of beta band to the SWO in DLS- (left) and DMS-MSNs (right) (Raylegh test, p<0.001 in both cases). Asterisk indicates the radial position of the beta peak. Beta peak occurs first in DMS-MSNs (p<0.001). **e,** Representative examples of beta phase locking in DLS- (left) and DMS- MSNs (right). White line represents the beginning of each Up state.

Direct and indirect MSNs have distinct properties in DLS and DMS.

We studied if MSNs spontaneous activity could be used to subdivide DLS and DMS into two additional circuits, corresponding to the direct or indirect pathway. Both types of MSNs were identified through the optopatcher[30] (Fig. 6a).

First, we analysed whether the features that were previously used to describe the SWO (Fig. 3) allowed us to differentiate between the MSNs belonging to each pathway in DLS and DMS. Our results show differences in the integration of the SWO between direct and indirect pathways only in the DLS. Specifically, we found three significant different features when comparing direct and indirect MSNs in the DLS: maximum and minimum voltage value of the Up state and the average value of the Up state (Fig. 6c). Despite these differences, when we tried to separate direct from indirect MSNs following the same approach previously used to classify MSNs belonging to the DLS and DMS (Fig. 3) [see Methods], it did not yield a clear separation of dMSNs and iMSNs. Classification accuracy was not better than chance (50%) for DMS-MSNs and 64% for DLS-MSNs (Fig. 6b).

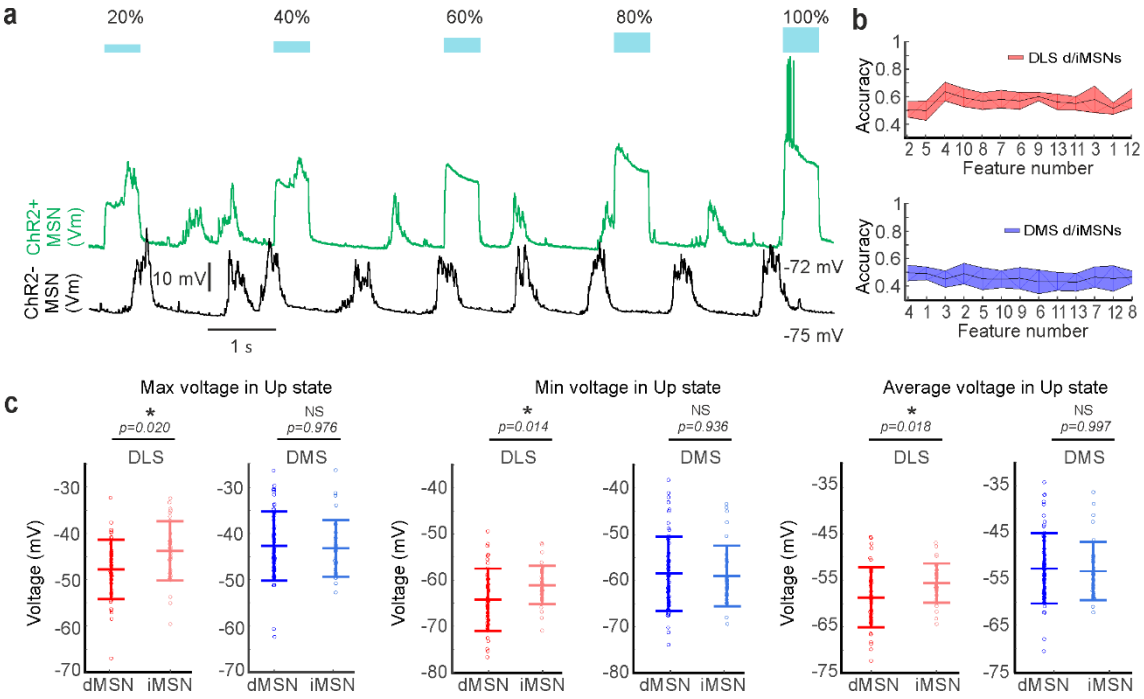

Figure 6. Differences between direct and indirect pathway MSNs in dorsal striatum. a, Example showing an *in vivo* identification of a MSN using the optopatcher. Responses in D2-ChR2-YFP mice (top trace, ChR2$^+$, green) to light pulses, inducing depolarization in the MSN. Negative cells (bottom trace, ChR2$^-$, black) did not respond to light pulses. Blue squares indicate the intensity of the light pulse stimulation, from 20 to 100 %. **b,** RFE to optimize the classification of dMSNs and iMSNs in DLS (red) or DMS (blue). A SVM with a linear kernel was selected as classification algorithm. **c,** Significant differences in three SWO features were found in DLS (red) between direct (dark) and indirect (light) pathways, but not in DMS (blue).

Finally, we analysed whether the differences in the intrinsic properties between DMS and DLS that we described previously (Table 1) were dependent on one of the two pathways. Resistance values, both during Up and Down states, were higher for indirect DLS-MSNs compared to indirect DMS-MSNs, while no differences were found between direct DLS- and DMS-MSNs.

In summary, even if the SWO features are not enough to subdivide DLS and DMS-MSNs in new categories related with the direct and indirect pathways, their differences in resistance and integration of the SWO demonstrate that they have particular properties along dorsal striatum.

		Input Resistance (MΩ)	Resistance Down state hyp. (MΩ)	Resistance Down state dep. (MΩ)	Resistance Up state hyp. (MΩ)	Resistance Up state dep. (MΩ)	Capacitance (pF)	Tau (ms)
DLS		**310± 25 ***	**291± 23 ***	**309± 23 ***	304± 23	312± 27	**26.65± 7.56 ***	4.57± 0.23
	dMSNs	291± 33	276± 31	279± 28	290± 29	292± 35	32.78± 12.81	4.52± 0.29
	iMSNs	**338± 41 #**	**312± 36 #**	**355± 40 #**	324± 37	342± 41	17.58± 2.35	4.63± 0.40
DMS		**255± 26 ***	**241± 25 ***	**259± 27 ***	262± 27	262± 27	**21.68± 2.26 ***	4.61± 0.48
	dMSNs	260± 22	249± 28	265± 23	269± 28	267± 23	23.20± 2.21	4.77± 0.19
	iMSNs	**241± 18 #**	**223± 18 #**	**248± 16 #**	248± 20	252± 20	18.43± 1.04	4.26± 0.24

Table 1. Intrinsic properties of DLS and DMS of direct and indirect MSNs. Comparisons between DLS- and DMS-MSNs ($p<0.05$, *****symbol). Comparisons between direct and indirect MSNs ($p<0.01$, **#** symbol). All values are means ± standard deviation.

DLS and DMS are two non-overlapping functional circuits in mouse.

Our results indicate that SWO features were enough to classify between DLS- and DMS-MSNs. Therefore, we used them to study the transition from one circuit to the other, exploring the properties of the SWO in dorsocentral striatum (DCS) (Fig. 7a), a hypothetical third region between DLS and DMS [see methods]. We considered three possible scenarios (Fig. 7a,b): If the activity of both circuits is mostly driven by the afferent inputs, we should observe a gradient moving from one circuit to the other (Hypothesis 1), or alternatively a third type of circuit (Hypothesis 2). Whether other factors, either extrinsic or intrinsic to the dorsal striatum, control the spontaneous activity of these circuits, we should observe a sharp transition from one circuit to the other (Hypothesis 3). To address this question, we recorded MSNs in the DCS [see methods] using *in vivo* whole-cell patch-clamp. As in the case of the DLS- and DMS-MSNs, we extracted 13 features of the SWO (Supplementary Table 2). Then we projected the DCS-MSNs into the standardized space used for the classification of DLS- and DMS-MSNs (Fig. 7c), containing the values of number of peaks, Up state amplitude and Up to Down transition slopes (Supplementary Table 2). In order to study the distribution of the DCS-MSNs along the classification boundary, we used the hypervector computed by the SVM to perform the classification (Fig. 7c, see methods). We projected the data onto this

hypervector and compared the distribution of the MSNs recorded from DCS to determine whether they belonged to either DLS or DMS circuits, or whether they had different properties (Fig. 7d). If a sharp functional boundary exists between DLS and DMS, we would have recorded an undetermined amount of MSNs belonging to both circuits (Hypothesis 3). Otherwise, it would appear a new cluster with an undescribed third functional type of MSN, with an unknown distribution along the hypervector (Hypothesis 2) or between DLS and DMS-MSNs distributions (Hypothesis 1). The distribution of MSNs recorded in the DCS was consistent with a mixture of MSNs from DLS and DMS circuits supporting a sharp functional boundary between DLS and DMS regions [see discussion]. DCS distribution (Fig. 7d, green trace) was significantly different to either the DLS and DMS distributions and equivalent to the combination of both (Fig. 7d, red, blue and black traces respectively). Thus, we conclude that all recorded MSNs in DS belong to the previously described DMS and DLS functional circuits.

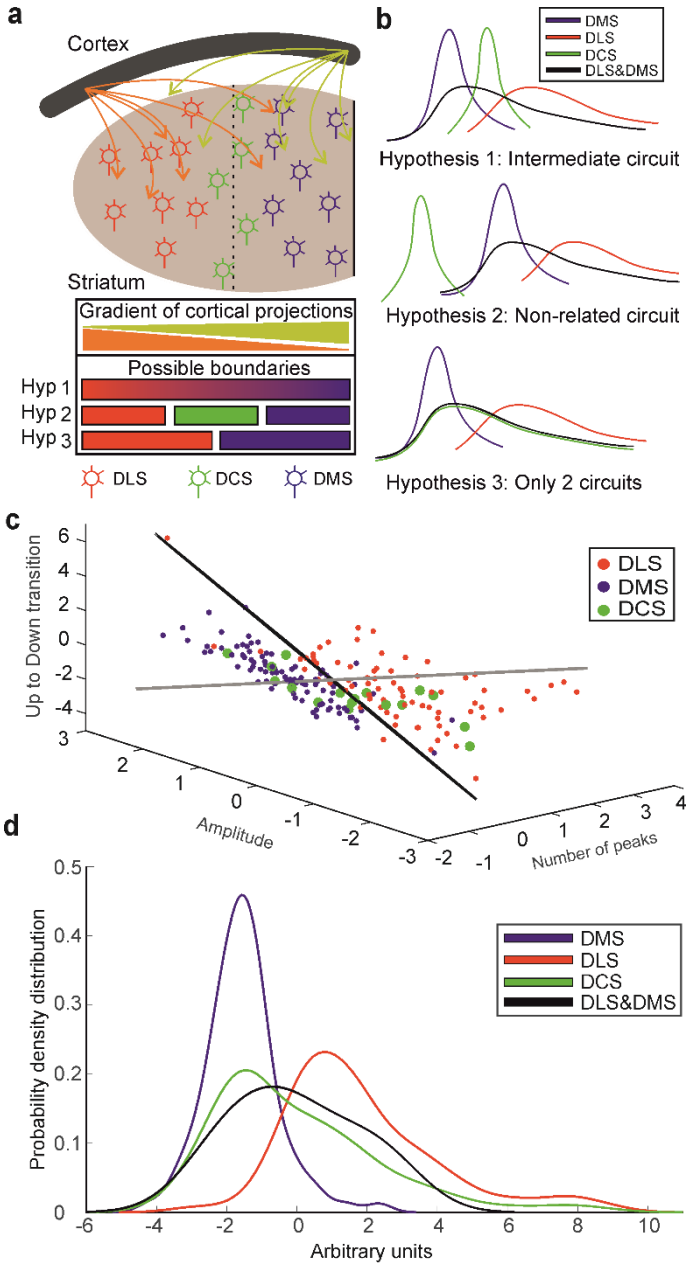

Figure 7. Study of the SWO in the DCS striatum and determination of the functional boundary between DLS and DMS. a, Schematic representation of the "boundary question". **b,** Three possible hypotheses about DCS-MSNs SWO. Hyp. 1: There is an intermediate distribution between DLS and DMS SWO (top); Hyp. 2: There is a different type of SWO distribution (middle); Hyp. 3: There is no specific DCS distribution of SWO and the MSNs recorded at DCS are a combination of DLS- and DMS-MSNs (bottom). The black line displays the distribution of the SWO recorded from both DLS and DMS **c,** Distribution of DLS-, DMS- and DCS-MSNs in the subspace of classification determined by the RFE. Classification plane in black. Orthogonal hypervector to the classification plane in grey. **d,** Distribution of dorsolateral, dorsomedial and dorsocentral MSNs along the orthogonal hypervector to the hyperplane classification. All comparison between distributions are significant ($p<0.01$) except for DCS with DMS+DLS ($p= 0.681$).

Discussion

Circuits are limited but not defined by their anatomy. In this study we have described two functional circuits in the anatomically homogenous DS, covering the medial and lateral regions, and separated by a sharp functional boundary. We discriminated DLS and DMS circuits based on different properties of their spontaneous activity under the SWO regime. We have demonstrated the presence of a sharp functional transition from one circuit to another in the central region of the dorsal striatum. This sharp transition is unexpected given the anatomical organization of corticostriatal projections, due to the profusion of axon terminals which provide overlapping inputs from multiple cortical areas to several regions of the dorsal striatum[13,5,7.] Hence, an essential question arises: why do we find a sharp boundary instead of a gradient transition between DLS- and DMS-MSNs?

Our results show that the number of peaks during Up states is an essential feature to discriminate between DLS- and DMS-MSNs (Fig. 3b) by the RFE, being higher in DLS-MSNs (Fig. 3a, feature 8). In order to understand this result, we recorded layer V neurons in FrA, M1, S1 and V1. Our results show larger number of peaks during Up states in FrA, M1, and S1 than in V1. This suggest that, in agreement with previous anatomical studies,[4,5,7], somatosensory-motor and premotor cortical regions exert sharper modulation onto the DLS-MSNs Up states than onto DMS-MSNs (Fig. 4c), which is more anatomically connected with visual, associative, and limbic prefrontal cortical areas[5]. We also observed a higher number of peaks between M1-S1 with respect to FrA (Fig. 4c). These results suggest that the temporal dynamics of the excitatory/inhibitory inputs during the SWO change between cortical areas and subsequently influence the striatum, opening an interesting question regarding the circuit mechanism underlying the observed cortical Up states differences.

Together with the cortical glutamatergic inputs, several additional factors may contribute to generate a functional boundary. Our classification reached ~90% of accuracy between DLS- and DMS-MSNs when the Up to Down state transition slopes were added (Fig. 3a,b, feature 12). Moreover, the Down to Up transition and transition ratio were both significantly different between DLS- and DMS-MSNs, as well (Fig. 3a, features 11 and 13 respectively). These data strongly suggest that Up states slopes are key elements to discriminate between dorsal striatal circuits. In order to better understand the slopes changes, we measured the time course of depolarized and hyperpolarized events of the SWO (Fig. 4d) and then compared them using the DH ratio (Fig. 4e). Cortical SWO propagates to MSNs but also to FS and ChI striatal interneurons[10]. FS interneurons provide strong feedforward inhibition to MSNs[14,31,32]. Previous reports demonstrated the presence of a FS gradient[15,33,34] or diverse types of PV interneurons with different electrophysiological properties[34,16] along the DS. Our results show more positive and negative ratio to the DMS-MSNs during the upward and downward SWO transitions slopes respectively, suggesting a different inhibitory recruitment in the DLS compared to DMS. Previous studies in cortex have shown that both upward and downward transition slopes are governed by $GABA_A$ and $GABA_B$ receptor activation[35,36]. Based on these evidences, and beyond the glutamatergic inputs, we hypothesize that PV interneurons may greatly influence the SWO of DLS-MSNs making them different from DMS ones.

In addition, other mechanisms can also contribute to the generation of a functional boundary; for instance, a similar scenario exists for ChI, which present a functional gradient with higher activity in the medial regions of the striatum[17,37]. ChI could modulate differently the SWO in DLS- and DMS-MSNs by disynaptic inhibition[38]. During the SWO under anaesthesia, dopaminergic neurons of the Substantia Nigra discharge spontaneous action potentials, in tonic or burst firing mode, uncorrelated with the cortical SWO cycle[39,]. This dopaminergic activity could induce different effects on the SWO in DLS- and DMS-MSNs, either directly mediated by different DA projections to DLS- and DMS-MSNs[39], or indirectly by their varied impact on ChI activity along the mediolateral axis[19]. Finally, it has been recently shown that SOM corticostriatal interneurons modulate the MSNs activity from motor cortical areas[40]. This type of interneuron could modulate the Up states transitions slopes directly, inhibiting the MSNs in their distal dendrites. Future work will have to determine whether FS, ChI, SOM or other types of interneurons and axonal projections contribute to the generation of this sharp functional transition.

SWO propagate along the cortical network[22]. As occurs in human slow-wave sleep[41], anesthetized mice exhibit a predominant pattern of SWO propagation from rostral to caudal brain poles[26]. Here, we show how the correlation and the probability of transition of an Up state from FrA is higher to the DLS, while a Up state recorded in V1 has higher probability to propagate to the DMS (Fig. 1h-i), suggesting a sequential activation of DMS and DLS, similar to the one between both poles of the cortex during the SWO. In order to test this hypothesis, we simultaneously recorded pairs of MSNs in DLS and DMS showing a similar probability of an Up state to appear in DLS before DMS (Fig. 2d) and to appear in FrA before V1. This description of the overall dynamics of corticostriatal connections is based on functional, rather than anatomical connectivity, supporting a stronger coupling of caudal, sensory related cortical regions to DMS, whereas premotor and motor frontal regions are more tightly connected to DLS. Consistent with this, the sequential activation of different striatal regions during a two-forced-decision-task has been recently reported[42]. DMS was first activated during the sensory stimulation period, followed by an increase in DLS activity coinciding with decision making and motor preparation/execution[42].

High frequency oscillations are usually associated with awake behavioural states. However, they also occur during the SWO in natural sleep, under anaesthesia[27] and in isolated cortical slices[23]. Especially relevant regarding the cortico-basal ganglia-thalamic loop are beta oscillations, which have been linked with the control of voluntary movements[28] and Parkinson's Disease[29]. Differences in Beta oscillations between caudate and putamen were reported in healthy monkeys at the end of a learned motor task[28]. We tested if beta or other high frequency bands could be relevant to discriminate between dorsal striatal regions. Our results did not show differences between DLS- and DMS-MSNs for theta and gamma bands (Supplementary Fig. 3), and only a difference in beta energy was detected (Fig. 5b), which was insufficient to discriminate between both dorsal striatal regions. Possible candidates to explain the observed higher beta power in DMS-MSNs are ChIs. This type of interneurons are more active in the DMS[17] and can facilitate

glutamate release from presynaptic terminals to the MSNs[37]. Thus, they might promote the fast glutamatergic transmission observed in DMS. Our work adds further detail to the description of this oscillation in healthy mice thanks to the use of NA-MEMD together with Hilbert transform (Fig. 1,4, Supplementary Fig. 1). Our results describing the differences between DLS and DMS in the Beta range may provide a new substrate for the study of aberrant beta oscillations in Parkinson disease. This result may indicate that the aberrant oscillations in Parkinson disease may be produced by the misbalance of normal striatal dynamics, as previously suggested[43].

Cortical inputs innervate the DS targeting both the direct and indirect pathway MSNs[13,44,10,30]. Both types of MSNs are co-activated during action initiation[45], and respond to tactile and visual stimulation[10]. However, a large number of studies described differences between direct and indirect MSNs in the DS[10,30,]. FS interneurons form more synaptic connections onto dMSNs[31,46], while iMSNs develop stronger synaptic connections onto dMSNs[46,47]. iMSNs have higher input resistance *in vitro*[48,49] and *in vivo*[10,30]. Recently, based on *in vivo* recordings of SWO in the DLS, it has been estimated that dMSNs receive stronger synaptic input than iMSNs[50]. Consequently, we studied if DLS and DMS could be further divided in two circuits belonging to direct and indirect pathways. To this end, we compared the SWO between the direct and indirect MSNs in both striatal regions. We found differences in the intrinsic properties of indirect MSNs (Table 1) and on the SWO features in the DLS, but not in the DMS (Fig. 6c). These results did not generate new categories, but demonstrate that direct and indirect pathways have distinct properties along dorsal striatum. This suggest that the interactions of the direct/indirect pathways may be different in DLS and DMS.

Based in the study of the SWO, we were able to: a) Unravel how cortico-striatal activity is propagated during a sequential cortical activation, and b) Identify specific dynamics of the information processing in the striatum. This approach can be extended to the study of any brain circuit, in order to uncover their circuit functional constrains. Hence, this kind of analysis is a sensible strategy to provide a level of understanding between anatomy and function when studying the brain.

In summary, we have shown how DLS and DMS are two non-overlapping circuits isolated by a sharp functional boundary. This work provides further understanding of the functional organization of the striatum and demonstrates that, consistent with the prediction of functional studies, the striatum is divided in two different regions. In addition, we have disclosed the functional coupling of these circuits to different cortical regions, based on the propagation and modulation of spontaneous activity. At last, we have discussed different possible mechanisms intrinsic to the striatal circuitry that may play a relevant role in the differentiation of DLS and DMS dynamics. Considering the relevance of the mouse striatum as a model for multiple human diseases, our results indicate that research will have to consider the idiosyncrasy of the two regions of the dorsal striatum.

Material and Methods

Ethical permit

All the experimental procedures were conformed to the directive 2010/63/EU of the European Parliament and of the Council, and the RD 53/2013 Spanish regulation on the protection of animals use for scientific purposes, approved by the government of the Autonomous Community of Valencia, under the supervision of the *Consejo Superior de Investigaciones Científicas* and the Miguel Hernandez University Committee for Animal use in Laboratory.

Animal model

D2-Cre (ER44 line, GENSAT) mouse line was crossed with the Channelrhodopsin (ChR2)-YFP reporter mouse line (Ai32, the Jackson laboratory) to induce expression of ChR2 in indirect MSNs and was used to perform optogenetic differentiation of direct (dMSN) and indirect (iMSNs) MSNs[30] while performing electrophysiological recordings in the striatum and some of the cortical recordings (33 mice for striatum, 1 mouse for cortex, 2 mice for paired recordings in the striatum). C57BL6 mice were used to perform the rest of the electrophysiological recordings of cortical neurons (n= 9).

Electrophysiological Recordings

Adult mice of both sexes (45 animals, 19 males and 26 females), between 12 and 44 weeks of age were used to perform the experiments (Supplementary Table 1). Anaesthesia was induced by intraperitoneal injection of ketamine (75 mg/kg) and medetomidine (1 mg/kg) diluted in 0.9% NaCl. A maintaining dose of ketamine (30 mg/kg i.m.) was administrated every 2 hours, after changes in the frequency of spontaneous activity recorded by cortical LFP or reflex responses to paw pinches. Tracheotomy was performed to increase mechanical stability during recordings by decreasing breathing related movements. Mice were placed in a stereotaxic device and air enriched with oxygen was delivered through a thin tube placed 1 cm from the tracheal cannula. Core temperature was monitored and maintained at 36.5 ± 0.5°C using a feedback-controlled heating pad (FHC Inc.). Craniotomies were drilled (S210, Camo) at seven sites for patch-clamp and extracellular recordings (from Bregma): AP 0 mm, L 2.5 mm (DMS); AP 0 mm, L 4 mm (DLS); AP 0 mm, L 3,25 mm (DCS); AP 2.7 mm, L 1 mm (FrA); AP 1.5 mm, L 2.0 mm (M1); AP −1.5 mm, L 3.25 mm (S1); AP −3.5 mm from Bregma, L 2.5 mm (V1) (following Paxinos and Franklin, 2001). When additional paired recordings were performed, the craniotomies were drilled at the following coordinates (from Bregma): AP 0 mm, L 1 mm (DMS); AP 0 mm, L 4 mm (DLS). Animals were sacrificed after recordings by injecting an overdose of sodium pentobarbital (200 mg/kg I.P.).

Whole-Cell Recordings

Whole-cell recordings were obtained from DLS, DMS, DCS between 2013-2647 µm and from layer V in FrA, M1, S1 and V1 at a depth of 675-926 µm. In detail, the number of neurons we recorded was: DLS (n= 77, from which dDLS= 49, iDLS= 34), DMS (n= 91, from which dDMS= 65, iDMS= 32), DCS (n= 17, from which dDCS= 10, iDCS= 7), and

in the layer V of frontal association cortex (FrA, n= 8), primary motor cortex (M1, n= 6), primary somatosensory cortex (S1, n= 6), and primary visual cortex (n= 6). Additional paired simultaneous whole-cell recordings of MSNs (n=6 pairs) were obtained from DLS and DMS between 2039-2348 µm of depth with two micromanipulators (Luigs & Neumann, MRE/MLE Mini 25). All of them in a perpendicular penetration angle of ~30º, except for DCS cells, in which the angle was ~20º. The exposed brain was continuously covered with 0.9% NaCl to prevent drying. Signals were amplified using MultiClamp 700B amplifier (Molecular Devices) and digitized at 20 kHz with a CED acquisition board and Spike 2 software (Cambridge Electronic Design). Borosilicate patch pipettes (1B150F-4, WPI), were pulled with a Flaming/Brown micropipette puller P-1000 (Sutter Instruments) and had an initial resistance of 6–12 MΩ. Pipettes were back-filled with intracellular solution containing: 125 mM K-gluconate, 10 mM KCl, 10 mM Na-Phosphocreatine, 10 mM HEPES, 4 mM ATP-Mg and 0.3 mM GTP-Na. pH and osmolarity were adjusted to ~7.4 and ~280 mOsm/L respectively. Biocytin (0.2-0.4 %, Sigma Aldrich) was then added to the intracellular solution to perform cell reconstruction after the experiment. To perform the analysis, 100 seconds of spontaneous activity (no current injection, no stimulation) were used from the recording. Input resistance (Table 1) was measured as the slope of a linear fit between injected depolarizing and hyperpolarizing current steps and membrane potential. Also, in order to improve the quantification of the described inward membrane rectification at hyperpolarized values of the MSNs membrane potentials, mean resistance in response to the negative and positive steps delivered at Up or Down states was also analysed (Table 1), as in Reig and Silberberg 2014[10].

Neurons having a deviation by more than 10 mV from their initial resting membrane potential were excluded from analysis. Only MSNs and cortical neurons were included in the data set.

Extracellular Recordings

Extracellular recordings were obtained using unipolar tungsten electrodes with impedance of 1 to 2 MΩ. The electrodes were placed in infragranular layers (~1000 µM depth from the pia) of two cortical regions in each experiment, from FrA, M1, S1, V1 cortex with an angle between 15° and 25°. Recordings were amplified using a differential AC Amplifier model 1700 (A-M Systems) and digitized at 20 KHz with CED and Spike-2, simultaneously with the whole-cell recording.

Optogenetic identification of *in vivo* recorded neurons

In order to identify "on line" the specific type of MSNs belonging to the direct (dMSNs) and indirect (iMSNs) pathways, the optopatcher was used[51,30,52] (A-M systems, WA USA). Controlled pulses (SLA-1000-2, two-channel universal LED driver, Mightex systems) of blue light (Fibre-coupled LED light source FCS-0470-000, 470 nm, Mightex systems) through Spike 2 software were delivered using an optic fibre (200 µm diameter, handmade) inserted into the patch-pipette, while recording their spontaneous activity (Fig. 6a). One or two serial pulses with 5 light steps of 500 ms each were delivered every 2 s with increasing intensity from 20 to 100 % of full LED power (minimal light intensity

was 0.166 mW; maximal intensity was 0.83 mW at the tip of the fibre). Power light was measured with an energy meter console (PM100D, Thorlabs). Positive cells responded to light pulses by depolarizing the membrane potential. Positive cells (Figure 6a, upper trace) responded within 2.69 ± 1.37 ms (ranging from 0.8 to 5 ms) to light pulses by a step-like depolarization of 13.3 ± 8.28 mV (ranging from 4 to 33 mV at maximal stimulation intensity), therefore were classified as iMSNs. Negative cells did not show any depolarization to light pulses (Figure 6a, bottom trace) and were classified as a putative dMSNs.

Morphological reconstruction

At the end of each experiment, mice were sacrificed with a lethal dose of sodium pentobarbital and perfused with a solution containing 4% paraformaldehyde in 0.1 M phosphate buffer (PB, pH 7.4). Brains were extracted and stored in PBS solution until the cutting. Before cutting, brains were transferred into PBS containing 30 % sucrose for at least 48 hours. Coronal slices (25 μm thick) containing the entire striatum from the recorded side (from AP 1.4 mm to AP -1.3 mm, following Paxinos and Franklin, 2001), were obtained using a digital automatic cryotome and collected on gelatine coated slides. Sections were incubated over night with Cy3-conjugated streptavidin (Jackson Immuno Research Laboratories) diluted (1:1000) in 1 % BSA, 0.3 % Triton-X 100 in 0.1 M PBS. Finally, the glass slides were covered with mowiol (Calbiochem) and imaged. Neurons were then reconstructed using a fluorescence microscope (DM 6000B, Leica) and a camera (DC350 FX, Leica).

SWO computation using NA-MEMD

We used Noise-assisted Multivariate Empirical Mode Decomposition (NA-MEMD) algorithm[53] together with Hilbert transform[54] for the analysis of oscillations both in LFPs and MSNS membrane potential. This algorithm is suited to decompose nonlinear nonstationary signals[55-58]. Given the well-known nonlinear properties of neural oscillations[59-62], the use of NA-MEMD leads to an increased detail of description when compared with traditional techniques[57,58,63]. In our knowledge is the first time that it is used to analyse membrane oscillations of single neurons. The original EMD[54] is a data driven algorithm suitable for nonlinear and non-stationary signals that does not rely on any predetermined template. It decomposes a given signal into a subset of oscillatory modes called Intrinsic Mode Functions (IMFs). Each IMF contains the oscillations of the original data in a certain frequency range. Then, Hilbert transform is applied onto each IMF in order to compute its instantaneous frequency and amplitude. The MEMD[64] is a multivariate extension of the original EMD to n-dimensional signals. The MEMD is computed simultaneously in all dimensions of the signal to ensure the same number of IMFs as output. In addition, new dimensions can be added to the data containing White Gaussian Noise (WGN) to increase its performance, as it has been described that WGN addition reduces mode mixing produced by signal intermittence[65], acting as a quasi-dyadic filter that enhances time frequency resolution[53,66]. The application of MEMD to the desired signal together with extra White Gaussian Noise dimensions is known as NA-

MEMD analysis[53]. EMDs algorithms plus Hilbert Transform have been increasingly used in neuroscience during the last years as they produce an enriched Time-Frequency (T-F) Spectrum when compared to traditional T-F linear tools[57,55]. In our work, we applied NA-MEMD algorithm to a multivariate signal composed by the intracellular recording, both LFPs and one extra WGN channel. By means of this analysis, we could warrant that the number of IMFs was the same in the intracellular and the LFPs recordings for a direct comparison of the SWO extracted using this method. In order to apply NA-MEMD analysis to our data, we adapted MEMD Matlab package (http://www.commsp.ee.ic.ac.uk/mandic/research/emd.htm). Standard stopping criterion was described elsewhere[67]. At last, we extracted the IMF carrying the SWO as the one with maximum correlation with the membrane voltage and visually confirmed it in all the recorded cells (Fig. 1c). Once we isolated the SWO of each recording using NA-MEMD, they were stored for further analysis.

Hilbert transform

We computed the frequency of the SWO, and theta (6-10 Hz), beta (10-20 Hz) and gamma (20-80 Hz) bands as the instantaneous frequency using the Hilbert transform[54]. For a given time series x(t), its Hilbert transform H(x)(t) is defined as:

$$H(x)(t) = \frac{1}{\pi} C \int_{-\infty}^{\infty} \frac{x(t')}{t-t'} dt'$$

where C indicates the Cauchy principal value. Hilbert transform results in a complex sequence with a real part which is the original data and an imaginary part which is a version of the original data with a 90° phase shift; this analytic signal is useful to calculate instantaneous amplitude and frequency; instantaneous amplitude is the amplitude of H(x)(t), instantaneous frequency is the time rate of change of the instantaneous phase angle.

Extraction of Up and Down states

In order to isolate Up and Down states from the membrane voltage we started by smoothing the trace using a 200 ms window. Then, we extracted the Up states using a threshold consisting of the mean value of the membrane potential (Vm) plus 0.5 standard deviations. Then, we merged the parts of fragmented Up states, detected as an interval shorter than 250 ms between the transition of a prospective Up state to a prospective Down state to the transition from a prospective Down state to a prospective Up state. Finally, detected Up states shorter than 200 ms where discarded.

When studying propagation of Up states, we considered two Up states from two different cortical regions, or a cortical LFP recording and an MSN to be part of the same SWO, thus propagating from one region to the other, when their onsets were closer in time than 500 ms.

Feature extraction of Up states

In order to describe the properties of the SWO of the recorded MSNs, we computed 13 parameters (Fig. 3a). First, we subtracted the IMFs carrying oscillations faster than 50 Hz from the MSNs membrane voltage recordings to eliminate the spikes. Then, we divided the trace into Up and Down states and calculated the mean (1), standard deviation (2), minimum (3) and maximum (4) values of the Up state. Additionally, we computed the peak to peak distance (5), which is the difference between the maximum and minimum values of the Up state, the maximum (6) and minimum (7) value of the Up state derivative and the number of peaks in the Up state (8), which described the presence of diplets or triplets in the Up state (Fig. 4a, b). To do so, we used the *findpeaks* Matlab function on the smoothed (200 ms smooth) Up state with a minimum peak height of 0.3 standard deviations and a minimum distance between peaks of 160 ms. We also computed the length (9), amplitude (10) and the speed of the transition from the Down to the Up state (11), and from the Up to the Down state (12) as well as the Slope transition ratio (13), which consisted of the magnitude of the Down to Up transition relative to the Up to Down transition. In order to measure the slopes, we first located the transition between states with a time window starting 100 ms before and lasting Up to 200 ms after the crossing point of the voltage threshold that was used to detect the Down and Up state (See above). Then, we smoothed (100 ms smooth) the selected region and computed its derivative. We delimited the transition between states computing the region over a threshold calculated as the mean plus 0.3 standard deviations of the derivative. Once we had delimited the transition, we fitted a lineal function to that region of the recording to compute the slope speed.

Detection of intracellular synaptic events

Intracellular synaptic currents were extracted using sharp deflections of the membrane voltage using a modification of the method presented here[23]. In brief, we applied a Parks-McClellan low-pass differentiator filter (order 20, cut off at 200 Hz) and computed the first derivative of the intracellular membrane voltage. Then, we extracted the temporal profile of depolarizing and hyperpolarizing events to the recorded cell using a threshold of the first derivative. We empirically determined a 2 standard deviations threshold to extract them. Next, we aligned the detected membrane deflections for both the hyperpolarizing and depolarizing events to the phase of the SWO as computed using NA-MEMD and normalized them to their respective maximum (Fig. 4e) in order to study the profile of the recruitment of excitation and inhibition during SWO. We computed the depolarizing/hyperpolarizing ratio subtracting the hyperpolarizing normalized value to the depolarizing one at each phase point.

For our whole-cell recordings, we have used a low-chloride intracellular solution (described above), in which the reversal potential for excitation is ~ -5 mV and $GABA_A$ inhibition ~ -70 mV. The average membrane potential during the Down states of the recorded MSNs was -69,2± 6,48 mV for DLS-MSNs and -69,31± 7,68 mV for DMS-MSNs. Around these voltages, the membrane fluctuations are depolarizing and excitatory. However, during the Up states (mean voltage values: -57,24± 6,34 mV for

DLS-MSNs and -52,95± 7,08 mV for DMS-MSNs), both depolarized and hyperpolarized events can be detected (Fig. 4d). As previously discussed here[23], this method does not extract all the EPSPs or IPSPs of the recorded cell, but it provides a major picture of the convergence of coordinated excitatory or inhibitory inputs onto the recorded cell that produced sharp deflections in the membrane voltage. Therefore, this method is sufficient to study the temporal profiles of hyper/depolarizing events onto the recorded cells during SWO.

Lateromedial classification

We classified MSNs from DLS and DMS using a Support Vector Machine (SVM) with a linear kernel. This supervised classification method estimates a hyperplane to separate both populations. Classification was cross-validated 10 times.

In order to determine which features were more relevant for the classification of DLS- and DMS-MSNs, we used Recursive Feature Elimination. This approach organizes the features relative to their importance to the classification by recursively pruning the least relevant features starting from the initial set.

MSNs distribution along the classification boundary

Support Vector Machines (SVMs) are supervised classifiers that predict the category of a new entry based on their previous training history and are not suitable to predict new categories in novel data. In order to study the spontaneous activity of DCS-MSNs, we examined its distribution in the classification space, relative to the classification boundary instead of directly using the output of a classifier. This approach provides information, not only about whether the new data (DCS-MSNs) creates a new cluster in the classification space, but also about where is it placed along the classification axis used to discriminate between DLS and DMS-MSNs. Hence, it provides a more informative approach to the distribution of DCS-MSNs relative to DLS and DMS-MSNs than a direct multi-category classification (i.e. discriminate versus Hypothesis 1 and 2, see results).

To calculate the distribution of the data along the classification boundary, we first obtained the coefficients and intersection values of the SVM used to classify the MSNs belonging to DLS and DMS. Once we obtained these parameters, we used them to project all data points to this hypervector and computed the probability density function of the new distributions (Fig. 7d). Now, the data was distributed along a single hypervector and we could compute the distribution of the MSNs along the classification boundary in a comprehensible manner to study the distribution of the DCS-MSNs.

Statistical analysis

All experimental comparisons were tested using the Wilcoxon Rank-sum test except stated otherwise. Directionality of the SWO from FrA in the cortex and DLS in the striatum was tested using Wilcoxon signed rank test. Phase locking of different frequency bands was tested using Rayleigh test. When required, alpha values for multiple comparisons were corrected using Holm-Bonferroni correction. Error bars presented in the graphs represent the standard deviation unless stated otherwise.

Acknowledgements

We thank Gilad Silberberg (Department of Neuroscience, Karolinska Institutet) for generous donation of D2-Cre(ChR2)-YFP mouse and for helping us to start-up the laboratory. We also want to thank Gilad Silberberg, Juan Lerma, Sandra Jurado, John F. Wesseling, Maya Ketzef, Cristina García-Frigola, Juan Pérez-Fernández and Roberto de la Torre for critical reading and discussions on this MS. J. A-C and M. S. are supported by the CSIC-Severo Ochoa Excellence Programme of the Instituto de Neurociencias [SEV-2013-0317]; R. M. is fellows by La Caixa-Severo Ochoa [2016/00006/001]. The study was supported by MINECO Fellowship [BES-2015-072187], Starting Grant I+D Jovenes Investigadores [BFU2014-60809-IN] and CSIC-Severo Ochoa Excellence Programmes of the Instituto de Neurociencias [SEV-2013-0317 and SEV-2017-0723].

References

1 Packard, M. G. & Knowlton, B. J. Learning and memory functions of the Basal Ganglia. *Annu Rev Neurosci* **25**, 563-593, doi:10.1146/annurev.neuro.25.112701.142937 (2002).

2 Graybiel, A. M. Habits, rituals, and the evaluative brain. *Annu. Rev. Neurosci.* **31**, 359-387 (2008).

3 Yin, H. H. & Knowlton, B. J. The role of the basal ganglia in habit formation. *Nat Rev Neurosci* **7**, 464-476, doi:10.1038/nrn1919 (2006).

4 Kincaid, A. E., Zheng, T. & Wilson, C. J. Connectivity and convergence of single corticostriatal axons. *Journal of Neuroscience* **18**, 4722-4731 (1998).

5 Hunnicutt, B. J. *et al.* A comprehensive excitatory input map of the striatum reveals novel functional organization. *Elife* **5**, e19103 (2016).

6 Doig, N. M., Moss, J. & Bolam, J. P. Cortical and thalamic innervation of direct and indirect pathway medium-sized spiny neurons in mouse striatum. *Journal of Neuroscience* **30**, 14610-14618 (2010).

7 Hooks, B. M. *et al.* Topographic precision in sensory and motor corticostriatal projections varies across cell type and cortical area. *Nat Commun* **9**, 3549, doi:10.1038/s41467-018-05780-7 (2018).

8 Hintiryan, H. *et al.* The mouse cortico-striatal projectome. *Nat Neurosci* **19**, 1100-1114, doi:10.1038/nn.4332 (2016).

9 Hauber, W. & Schmidt, W. J. Differential effects of lesions of the dorsomedial and dorsolateral caudate-putamen on reaction time performance in rats. *Behav Brain Res* **60**, 211-215, doi:10.1016/0166-4328(94)90149-x (1994).

10 Reig, R. & Silberberg, G. Multisensory integration in the mouse striatum. *Neuron* **83**, 1200-1212 (2014).

11 Hilário, M. R. & Costa, R. M. High on habits. *Frontiers in neuroscience* **2**, 30 (2008).

12 Flaherty, A. W. & Graybiel, A. Corticostriatal transformations in the primate somatosensory system. Projections from physiologically mapped body-part representations. *Journal of Neurophysiology* **66**, 1249-1263 (1991).

13 Wall, N. R., De La Parra, M., Callaway, E. M. & Kreitzer, A. C. Differential innervation of direct-and indirect-pathway striatal projection neurons. *Neuron* **79**, 347-360 (2013).

14 Tepper, J. M., Wilson, C. J. & Koós, T. Feedforward and feedback inhibition in neostriatal GABAergic spiny neurons. *Brain research reviews* **58**, 272-281 (2008).

15 Gerfen, C. R., Baimbridge, K. G. & Miller, J. J. The neostriatal mosaic: compartmental distribution of calcium-binding protein and parvalbumin in the basal ganglia of the rat and monkey. *Proceedings of the National Academy of Sciences* **82**, 8780-8784 (1985).

16 Muñoz-Manchado, A. B. *et al.* Diversity of interneurons in the dorsal striatum revealed by single-cell RNA sequencing and PatchSeq. *Cell reports* **24**, 2179-2190. e2177 (2018).
17 Matamales, M., Götz, J. & Bertran-Gonzalez, J. Quantitative imaging of cholinergic interneurons reveals a distinctive spatial organization and a functional gradient across the mouse striatum. *PloS one* **11**, e0157682 (2016).
18 Ikemoto, S. Dopamine reward circuitry: two projection systems from the ventral midbrain to the nucleus accumbens–olfactory tubercle complex. *Brain research reviews* **56**, 27-78 (2007).
19 Chuhma, N. *et al.* Dopamine neuron glutamate cotransmission evokes a delayed excitation in lateral dorsal striatal cholinergic interneurons. *Elife* **7**, e39786 (2018).
20 Getting, P. A. Emerging principles governing the operation of neural networks. *Annual review of neuroscience* **12**, 185-204 (1989).
21 Luczak, A., McNaughton, B. L. & Harris, K. D. Packet-based communication in the cortex. *Nature Reviews Neuroscience* **16**, 745-755 (2015).
22 Sanchez-Vives, M. V., Massimini, M. & Mattia, M. Shaping the Default Activity Pattern of the Cortical Network. *Neuron* **94**, 993-1001, doi:10.1016/j.neuron.2017.05.015 (2017).
23 Compte, A. *et al.* Spontaneous high-frequency (10–80 Hz) oscillations during up states in the cerebral cortex in vitro. *Journal of Neuroscience* **28**, 13828-13844 (2008).
24 Reig, R. & Silberberg, G. Distinct Corticostriatal and Intracortical Pathways Mediate Bilateral Sensory Responses in the Striatum. *Cereb Cortex* **26**, 4405-4415, doi:10.1093/cercor/bhw268 (2016).
25 Wilson, C. J. & Kawaguchi, Y. The origins of two-state spontaneous membrane potential fluctuations of neostriatal spiny neurons. *Journal of neuroscience* **16**, 2397-2410 (1996).
26 Ruiz-Mejias, M., Ciria-Suarez, L., Mattia, M. & Sanchez-Vives, M. V. Slow and fast rhythms generated in the cerebral cortex of the anesthetized mouse. *Journal of neurophysiology* **106**, 2910-2921 (2011).
27 Steriade, M., Amzica, F. & Contreras, D. Synchronization of fast (30-40 Hz) spontaneous cortical rhythms during brain activation. *J Neurosci* **16**, 392-417 (1996).
28 Feingold, J., Gibson, D. J., DePasquale, B. & Graybiel, A. M. Bursts of beta oscillation differentiate postperformance activity in the striatum and motor cortex of monkeys performing movement tasks. *Proceedings of the National Academy of Sciences* **112**, 13687-13692 (2015).
29 Brown, P. Oscillatory nature of human basal ganglia activity: relationship to the pathophysiology of Parkinson's disease. *Mov Disord* **18**, 357-363, doi:10.1002/mds.10358 (2003).
30 Ketzef, M. *et al.* Dopamine depletion impairs bilateral sensory processing in the striatum in a pathway-dependent manner. *Neuron* **94**, 855-865. e855 (2017).
31 Gittis, A. H., Nelson, A. B., Thwin, M. T., Palop, J. J. & Kreitzer, A. C. Distinct roles of GABAergic interneurons in the regulation of striatal output pathways. *Journal of Neuroscience* **30**, 2223-2234 (2010).
32 Szydlowski, S. N. *et al.* Target selectivity of feedforward inhibition by striatal fast-spiking interneurons. *Journal of Neuroscience* **33**, 1678-1683 (2013).
33 Kita, H., Kosaka, T. & Heizmann, C. Parvalbumin-immunoreactive neurons in the rat neostriatum: a light and electron microscopic study. *Brain research* **536**, 1-15 (1990).
34 Monteiro, P. *et al.* Dichotomous parvalbumin interneuron populations in dorsolateral and dorsomedial striatum. *The Journal of physiology* **596**, 3695-3707 (2018).
35 Sanchez-Vives, M. V. *et al.* Inhibitory modulation of cortical up states. *Journal of neurophysiology* **104**, 1314-1324 (2010).
36 Perez-Zabalza, M. *et al.* Modulation of cortical slow oscillatory rhythm by GABAB receptors: an experimental and computational study. *bioRxiv*, 2019.2012.2014.866442, doi:10.1101/2019.12.14.866442 (2019).

37 Abudukeyoumu, N., Hernandez-Flores, T., Garcia-Munoz, M. & Arbuthnott, G. W. Cholinergic modulation of striatal microcircuits. *European Journal of Neuroscience* **49**, 604-622 (2019).
38 English, D. F. *et al.* GABAergic circuits mediate the reinforcement-related signals of striatal cholinergic interneurons. *Nature neuroscience* **15**, 123 (2012).
39 Brown, M. T., Henny, P., Bolam, J. P. & Magill, P. J. Activity of neurochemically heterogeneous dopaminergic neurons in the substantia nigra during spontaneous and driven changes in brain state. *Journal of Neuroscience* **29**, 2915-2925 (2009).
40 Melzer, S. *et al.* Distinct Corticostriatal GABAergic Neurons Modulate Striatal Output Neurons and Motor Activity. *Cell Rep* **19**, 1045-1055, doi:10.1016/j.celrep.2017.04.024 (2017).
41 Massimini, M., Huber, R., Ferrarelli, F., Hill, S. & Tononi, G. The sleep slow oscillation as a traveling wave. *Journal of Neuroscience* **24**, 6862-6870 (2004).
42 Peters, A. J., Steinmetz, N. A., Harris, K. D. & Carandini, M. Striatal activity reflects cortical activity patterns. *bioRxiv*, 703710 (2019).
43 McCarthy, M. *et al.* Striatal origin of the pathologic beta oscillations in Parkinson's disease. *Proceedings of the National Academy of Sciences* **108**, 11620-11625 (2011).
44 Kress, G. J. *et al.* Convergent cortical innervation of striatal projection neurons. *Nature neuroscience* **16**, 665 (2013).
45 Cui, G. *et al.* Concurrent activation of striatal direct and indirect pathways during action initiation. *Nature* **494**, 238 (2013).
46 Planert, H., Szydlowski, S. N., Hjorth, J. J., Grillner, S. & Silberberg, G. Dynamics of synaptic transmission between fast-spiking interneurons and striatal projection neurons of the direct and indirect pathways. *Journal of Neuroscience* **30**, 3499-3507 (2010).
47 Taverna, S., Ilijic, E. & Surmeier, D. J. Recurrent collateral connections of striatal medium spiny neurons are disrupted in models of Parkinson's disease. *Journal of Neuroscience* **28**, 5504-5512 (2008).
48 Gertler, T. S., Chan, C. S. & Surmeier, D. J. Dichotomous anatomical properties of adult striatal medium spiny neurons. *Journal of Neuroscience* **28**, 10814-10824 (2008).
49 Planert, H., Berger, T. K. & Silberberg, G. Membrane properties of striatal direct and indirect pathway neurons in mouse and rat slices and their modulation by dopamine. *PloS one* **8**, e57054 (2013).
50 Filipović, M. *et al.* Direct pathway neurons in mouse dorsolateral striatum in vivo receive stronger synaptic input than indirect pathway neurons. *Journal of Neurophysiology* **122**, 2294-2303, doi:10.1152/jn.00481.2019 (2019).
51 Katz, Y., Yizhar, O., Staiger, J. & Lampl, I. Optopatcher—an electrode holder for simultaneous intracellular patch-clamp recording and optical manipulation. *Journal of neuroscience methods* **214**, 113-117 (2013).
52 Katz, Y., Sokoletsky, M. & Lampl, I. In-vivo optogenetics and pharmacology in deep intracellular recordings. *Journal of neuroscience methods*, 108324 (2019).
53 Ur Rehman, N. & Mandic, D. P. Filter bank property of multivariate empirical mode decomposition. *IEEE transactions on signal processing* **59**, 2421-2426 (2011).
54 Huang, N. E. *et al.* The empirical mode decomposition and the Hilbert spectrum for nonlinear and non-stationary time series analysis. *Proceedings of the Royal Society of London. Series A: Mathematical, Physical and Engineering Sciences* **454**, 903-995 (1998).
55 Hu, M. & Liang, H. Search for information-bearing components in neural data. *PLoS One* **9**, e99793 (2014).
56 Mandic, D. P., ur Rehman, N., Wu, Z. & Huang, N. E. Empirical mode decomposition-based time-frequency analysis of multivariate signals: The power of adaptive data analysis. *IEEE signal processing magazine* **30**, 74-86 (2013).
57 Alegre-Cortés, J. *et al.* Time–frequency analysis of neuronal populations with instantaneous resolution based on noise-assisted multivariate empirical mode decomposition. *Journal of neuroscience methods* **267**, 35-44 (2016).

58 Alegre-Cortés, J. *et al.* Toward an Improvement of the Analysis of Neural Coding. *Frontiers in neuroinformatics* **11**, 77 (2018).
59 Laurent, G. Dynamical representation of odors by oscillating and evolving neural assemblies. *Trends Neurosci* **19**, 489-496, doi:10.1016/S0166-2236(96)10054-0 (1996).
60 Averbeck, B. B., Latham, P. E. & Pouget, A. Neural correlations, population coding and computation. *Nat Rev Neurosci* **7**, 358-366, doi:10.1038/nrn1888 (2006).
61 Shamir, M. & Sompolinsky, H. Nonlinear population codes. *Neural Comput* **16**, 1105-1136, doi:10.1162/089976604773717559 (2004).
62 Cole, S. R. & Voytek, B. Brain Oscillations and the Importance of Waveform Shape. *Trends Cogn Sci* **21**, 137-149, doi:10.1016/j.tics.2016.12.008 (2017).
63 Hu, M. & Liang, H. Noise-assisted instantaneous coherence analysis of brain connectivity. *Computational intelligence and neuroscience* **2012** (2012).
64 Rehman, N. & Mandic, D. P. Multivariate empirical mode decomposition. *Proceedings of the Royal Society A: Mathematical, Physical and Engineering Sciences* **466**, 1291-1302 (2009).
65 Wu, Z. & Huang, N. E. Ensemble empirical mode decomposition: a noise-assisted data analysis method. *Advances in adaptive data analysis* **1**, 1-41 (2009).
66 Flandrin, P., Rilling, G. & Goncalves, P. Empirical mode decomposition as a filter bank. *IEEE signal processing letters* **11**, 112-114 (2004).
67 Rilling, G., Flandrin, P. & Goncalves, P. in *IEEE-EURASIP workshop on nonlinear signal and image processing.* 8-11 (NSIP-03, Grado (I)).

SUPPLEMENTARY INFORMATION

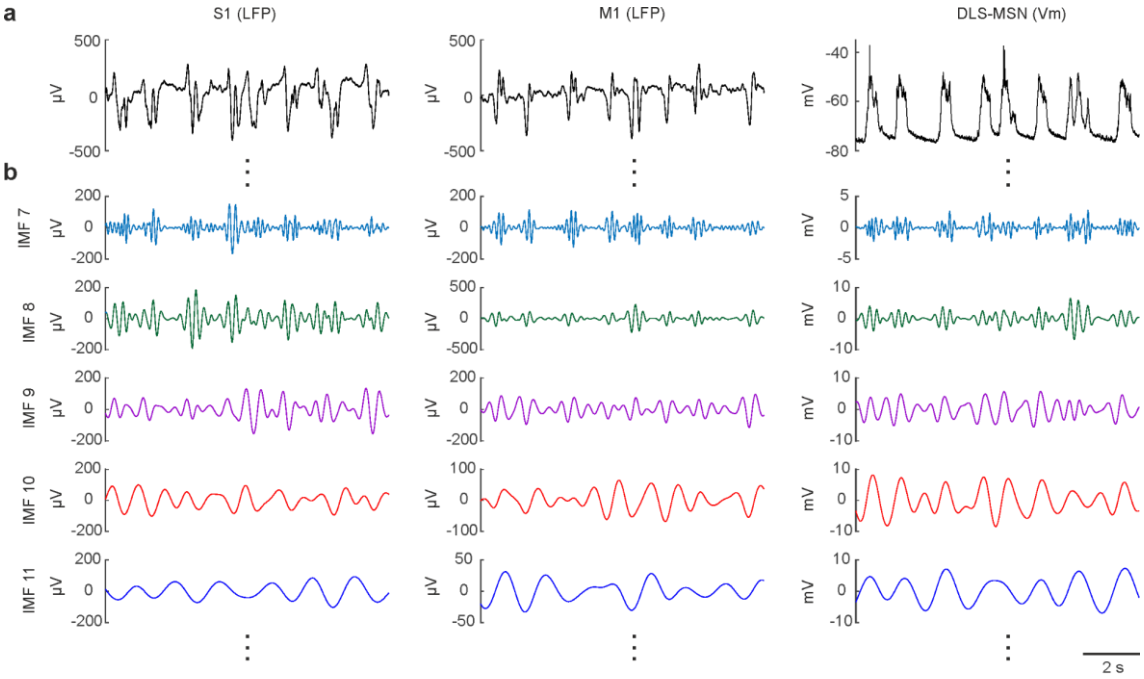

Supplementary Figure 1. Example of decomposition of different traces by the NA-MEMD. **a,** Example traces of a S1 LFP (left), M1 LFP (center) and a whole-cell recording in DLS (right). **b,** Consecutive IMFs obtained by applying NA-MEMD to the signals in a, starting from the 7th IMF. The IMF classifies the oscillatory activity from the fastest to the slowest.

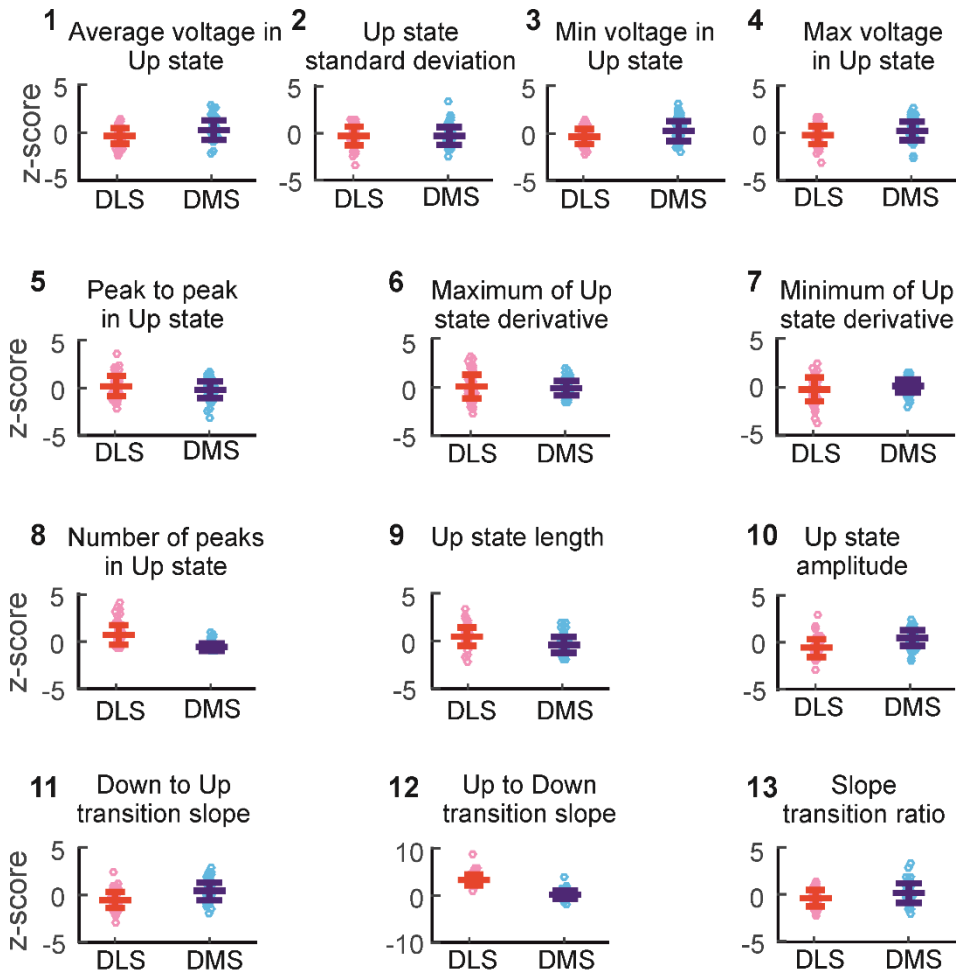

Supplementary Figure 2. Z-scoring of the SWO features. Z-score transformation of the computed features of the SWO that were used for the classification of DLS- and DMS-MSNs in figure 3a. P values are the same as in figure 3a.

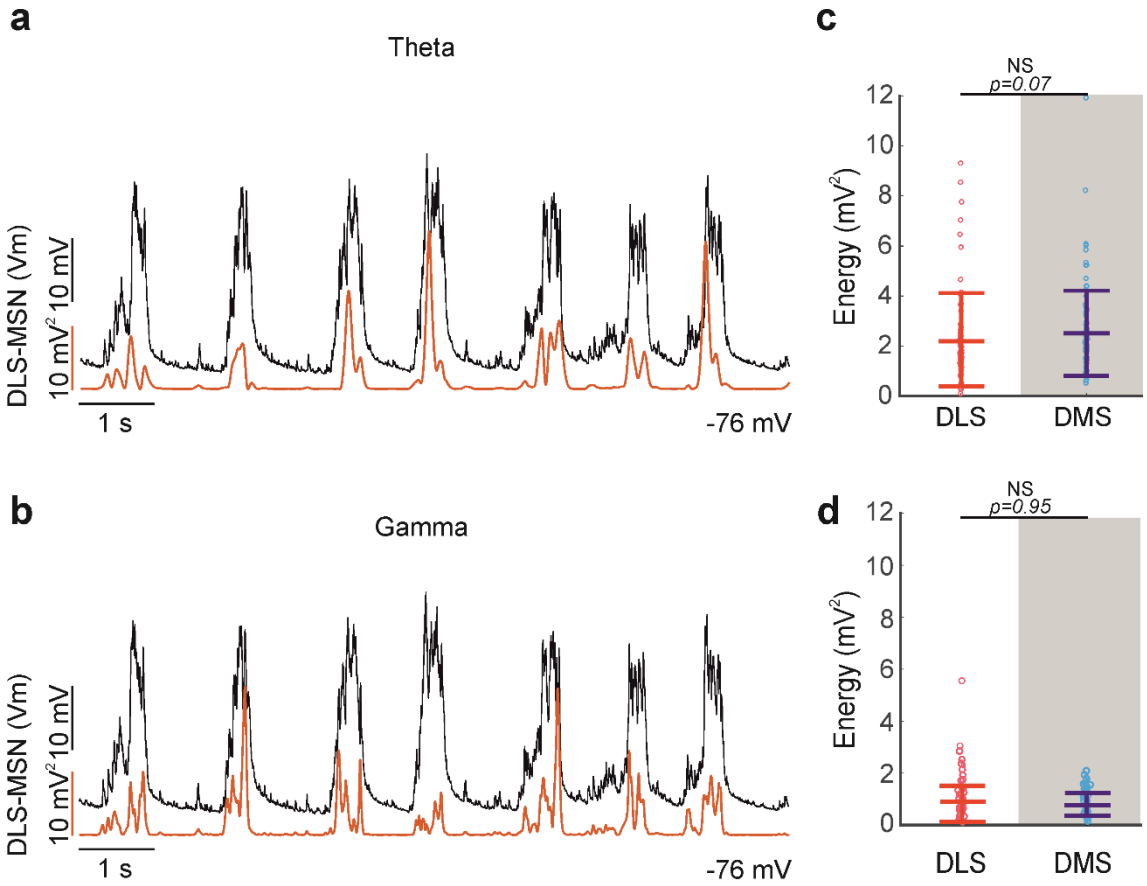

Supplementary Figure 3. Theta and Gamma band in membrane voltage of dorsal striatum. a, Representative example of the energy of the theta band (orange trace) of a DLS-MSN during SWO regime. **b,** Representative example of the energy of the Gamma band (red trace) of a DLS-MSN during SWO regime. **c,** Energy of the Theta band of DLS- and DMS-MSNs. **d,** Energy of the Gamma band of DLS and DMS-MSNs. Same neuron in a and b.

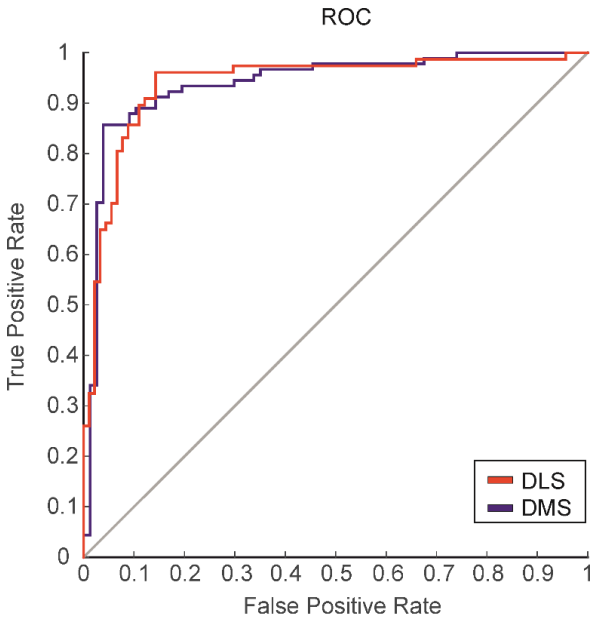

Supplementary Figure 4. ROC curve for the classification using one-animal-out strategy. We independently classified the MSNs of each animal training the classifier using the rest of the dataset to exclude any possible inter-animal bias during training.

Animals	Males	Females	Weight (gr)	Male weight (gr)	Female weight (gr)	Age (weeks)	Male age (weeks)	Female age (weeks)	Cells/animal	Cells/male	Cells/female
45	19	26	33.54±1.37	30.04±1.58	37.78±1.94	24.66±1.31	22.52±1.79	27.26±1.84	4.38±0.49	4±0.92	4.69±0.39

Supplementary Table 1. Data set description. The three first columns show total values, the rest show means ± standard deviation.

Feature	Mean value
1- Average voltage in Up state (mV)	-54.44 ± 6.28
2- Up state standard deviation (mV)	5.32 ± 1.36
3- Min voltage in Up state (mV)	-59.95 ± 6.23
4- Max voltage in Up state (mV)	-43.99 ± 6.20
5- Peak to peak in Up state (mV)	20.74 ± 4.65
6- Maximum of Up state derivative (dmV/dt)	0.65 ± 0.14
7- Minimum of Up state derivative (dmV/dt)	-0.512 ± 0.12
8- Number of peaks in Up state (units)	1.20 ± 0.15
9- Up state length (ms)	431.40 ± 71.50
10- Up state amplitude (mV)	13.62 ± 4.10
11- Down to Up transition slope (mV/s x 10^2)	0.829 ± 0.25
12- Up to Down transition slope (mV/s x 10^2)	0.514 ± 0.13
13- Slope transition ratio (arbitrary units)	1.61 ± 0.36

Supplementary Table 2. Featurization of the SWO of the DCS-MSNs. The number preceding the feature labels are the same as the ones showed in figure 3. All values display means ± standard deviation.